UC Irvine
UC Irvine Previously Published Works

Title

Squid leucophore-inspired engineering of optically dynamic human cells

Permalink

https://escholarship.org/uc/item/9xt172vj

Journal

iScience, 26(7)

ISSN

2589-0042

Authors

Bogdanov, Georgii

Chatterjee, Atrouli

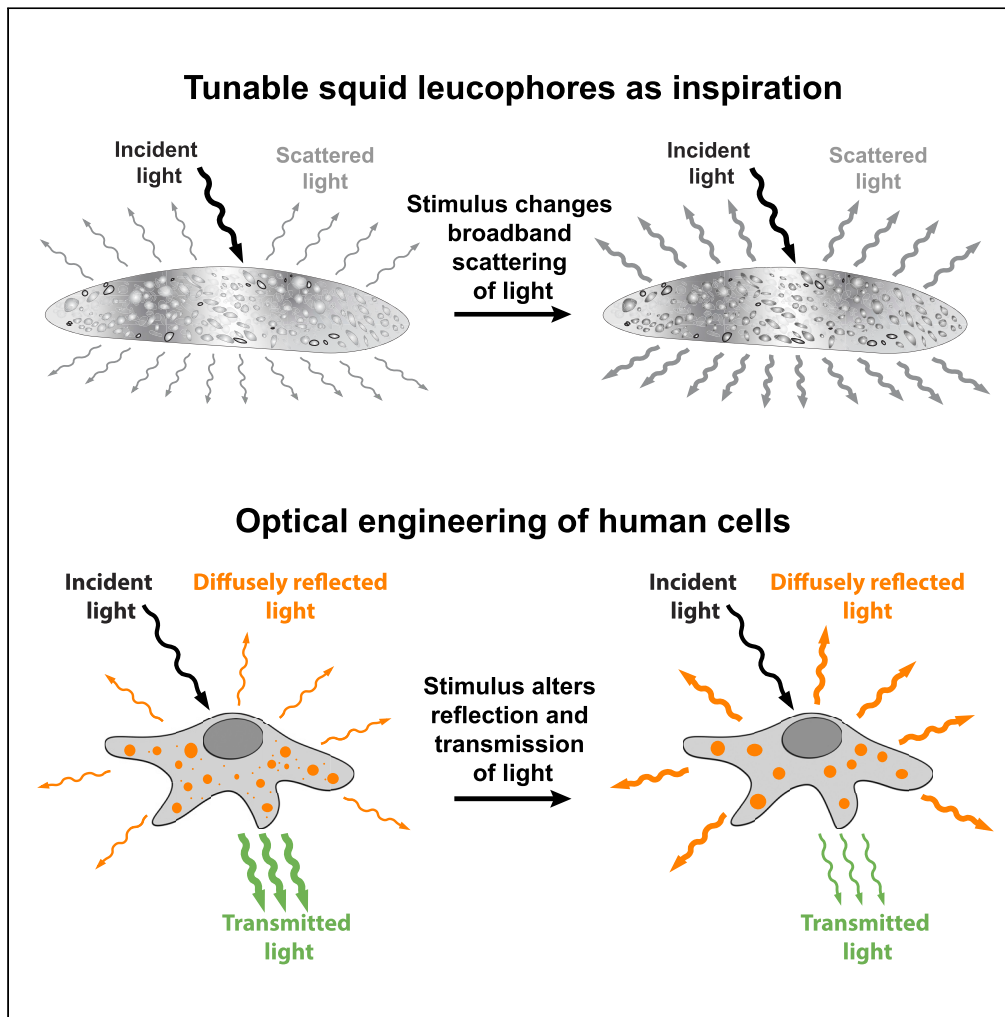Makeeva, Nataliya

et al.

Publication Date

2023-07-01

DOI

10.1016/j.isci.2023.106854

Peer reviewed

Article

Squid leucophore-inspired engineering of optically dynamic human cells

Tunable squid leucophores as inspiration

Incident light · Scattered light

Stimulus changes broadband scattering of light

Incident light · Scattered light

Optical engineering of human cells

Incident light · Diffusely reflected light

Stimulus alters reflection and transmission of light

Transmitted light

Incident light · Diffusely reflected light

Transmitted light

Georgii Bogdanov, Atrouli Chatterjee, Nataliya Makeeva, Aleeza Farrukh, Alon A. Gorodetsky

alon.gorodetsky@uci.edu

Highlights
Optical engineering

Cephalopod-inspired systems

Holotomographic imaging

Article

Squid leucophore-inspired engineering of optically dynamic human cells

Georgii Bogdanov,[1] Atrouli Chatterjee,[1] Nataliya Makeeva,[2] Aleeza Farrukh,[1] and Alon A. Gorodetsky[1,3,4,5,*]

SUMMARY

Cephalopods (e.g., squids, octopuses, and cuttlefishes) possess remarkable dynamic camouflage abilities and therefore have emerged as powerful sources of inspiration for the engineering of dynamic optical technologies. Within this context, we have focused on the development of engineered living systems that can emulate the tunable optical characteristics of some squid skin cells. Herein, we expand our ability to controllably incorporate reflectin-based structures within mammalian cells via genetic engineering methods, and demonstrate that such structures can facilitate holotomographic and standard microscopy imaging of the cells. Moreover, we show that the reflectin-based structures within our cells can be reconfigured with a straightforward chemical stimulus, and we quantify the stimulus-induced changes observed for the structures at the single cell level. The reported findings may enable a better understanding of the color- and appearance-changing capabilities of some cephalopod skin cells and could afford opportunities for reflectins as molecular probes in the fields of cell biology and biomedical optics.

INTRODUCTION

Cephalopods, such as squid, octopuses, and cuttlefishes, are renowned for their remarkable dynamic color- and appearance-changing capabilities.[1–3] As one example, the female *Doryteuthis opalescens* squid possesses a dorsal mantle stripe that can be switched between nearly transparent and completely opaque, i.e., bright white[4] (Figure 1A). These tissue-level appearance changes arises from tunable diffusely reflecting cells (leucophores), which contain disordered arrangements of particles (leucosomes) consisting of a high refractive index protein called reflectin (Figure 1B).[3–7] For such leucophores, the application of an external chemical stimulus (acetylcholine) to the stripe has been proposed to reconfigure the assembly state of reflectin within the leucosomes and thus to correspondingly alter the scattering of light by the cells (Figures 1B).[4,6] Given such unique abilities, it is hardly surprising that the *D. opalescens* squid (and other cephalopods) have emerged as powerful sources of inspiration for the engineering of dynamic optical technologies.[8–14]

Within our laboratory, we have focused on the development of engineered living systems that can emulate the tunable optical characteristics of some cephalopod skin cells.[15] To achieve this goal, we initially demonstrated the adhesion, proliferation, and differentiation of mammalian stem cells on reflectin films and accordingly validated the excellent biocompatibility of this protein.[16,17] We subsequently genetically engineered mammalian cells for the formation of high-contrast reflectin-based structure arrangements (architectures) within their interiors and observed that the cells featured high average refractive indices of $\gtrapprox 1.42$ via quantitative phase microscopy techniques (Figure 1C).[15] We furthermore showed that the application of an external chemical stimulus (specifically, sodium chloride) could tune the extent of light scattering and the transparency for our genetically engineered cells, presumably by reconfiguring their internalized structure arrangements (Figure 1C).[15] However, in our prior work, we did not engineer mammalian cells for the stable rather than transient expression of reflectin, leverage the properties of the subcellular reflectin-based structures for routine biological assays, or confirm the mechanisms underpinning our reflectin-expressing cells' tunable light-scattering functionalities.

Herein, we establish a powerful and synergistic combination of methodologies for incorporating, interrogating, and controlling reflectin-based structures in mammalian cells. First, we demonstrate genetic engineering of mammalian cells for both the transient and stable expression of reflectin and characterize the

[1]Department of Chemical and Biomolecular Engineering, University of California, Irvine, Irvine, CA 92697, USA

[2]Department of Biomedical Engineering, University of California, Irvine, Irvine, CA 92697, USA

[3]Department of Chemistry, University of California, Irvine, Irvine, CA 92697, USA

[4]Department of Materials Science and Engineering, University of California, Irvine, Irvine, CA 92697, USA

[5]Lead contact

*Correspondence:
alon.gorodetsky@uci.edu
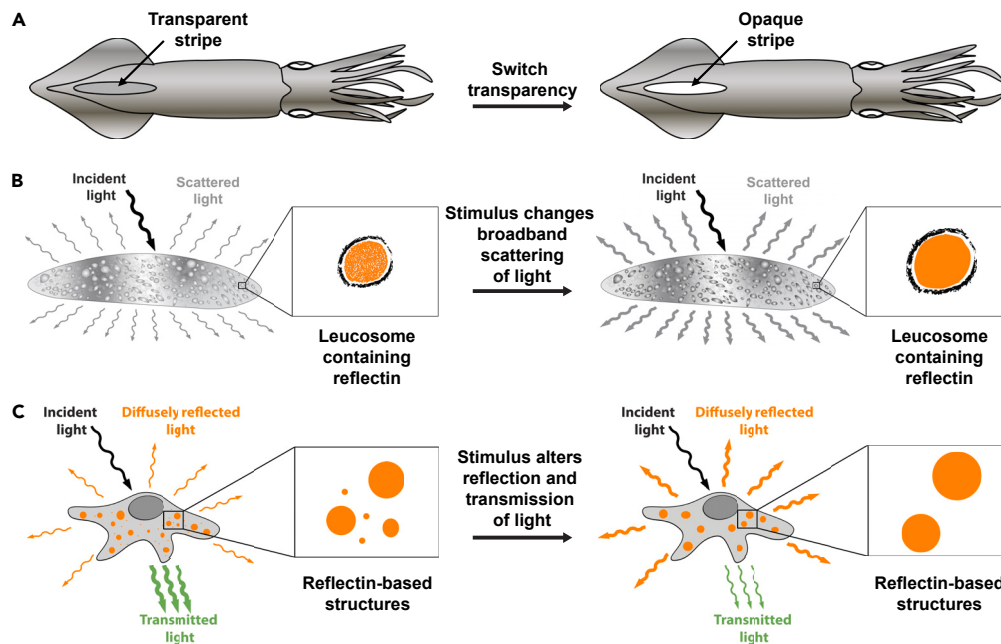https://doi.org/10.1016/j.isci.2023.106854

Figure 1. Overview of the female squid as biological inspiration and the engineering of optically dynamic mammalian cells

(A) An illustration of a female *Doryteuthis opalescens* squid, which switches a stripe on its mantle from transparent to opaque.

(B) An illustration of a tunable leucophore, for which the application of a chemical stimulus was proposed to reconfigure the assembly state of reflectin within the leucosomes and thus change the broadband scattering of light.

(C) A schematic of engineered human cells containing reflectin-based structures, for which the application of a chemical stimulus was proposed to reconfigure the aggregation state of the structures and thus alter the cells' diffuse transmission and reflection of light.

reflectin-based structures formed within the cells with holotomography, which is a microscopy technique for imaging whole cells in three dimensions (Figure S1). In tandem, we prove that the high contrast structures formed within the engineered cells can facilitate brightfield microscopy imaging during standard cell migration assays, which are ubiquitous in the biological sciences. Second, we demonstrate that the reflectin-based structures within our transiently and stably transfected cells can be reconfigured with a straightforward chemical stimulus. Concomitantly, we quantify the stimulus-induced changes in the numbers, refractive indices, and size distributions of the subcellular structures at the single-cell level. The combined findings underscore the value of reflectin-expressing mammalian cells as platforms for fundamentally understanding the optical properties of squid skin cells and also suggest that reflectin proteins are promising genetically encoded reporters for advanced optical imaging applications.

RESULTS

Genetic control over the optical properties of human cells

We began our efforts by forming and visualizing reflectin-based architectures within transiently transfected human cells (Figure 2A). For this purpose, we cultured human embryonic kidney (HEK) 293 cells that transiently expressed the *Doryteuthis pealeii* reflectin A1 isoform (RfA1)[15] and characterized such cells with a combination of holotomography, phase contrast microscopy, fluorescence microscopy, and immunofluorescence microscopy techniques (see STAR Methods).[15,18–21] First, the representative phase images revealed the presence of light-scattering arrangements comprised of spheroidal structures within the cells (Figure 2B). Second, the corresponding holotomographic refractive index maps indicated that such spheroidal structures consisted of RfA1 because of their higher refractive indices relative to the surrounding cytoplasm and organelles (Figure 2C and Videos S1 and S2). Third, the complementary phase contrast microscopy monitoring and cell viability assays showed that the cells featured epithelial-like morphologies and viabilities that typically exceeded 96%, even after undergoing 24 h of continuous fluorescence/phase contrast imaging (Figures S2 and S3). Fourth, the immunofluorescence images obtained for fixed transiently transfected cells further confirmed the presence of expressed RfA1 (Figure S4). Here, the analogous
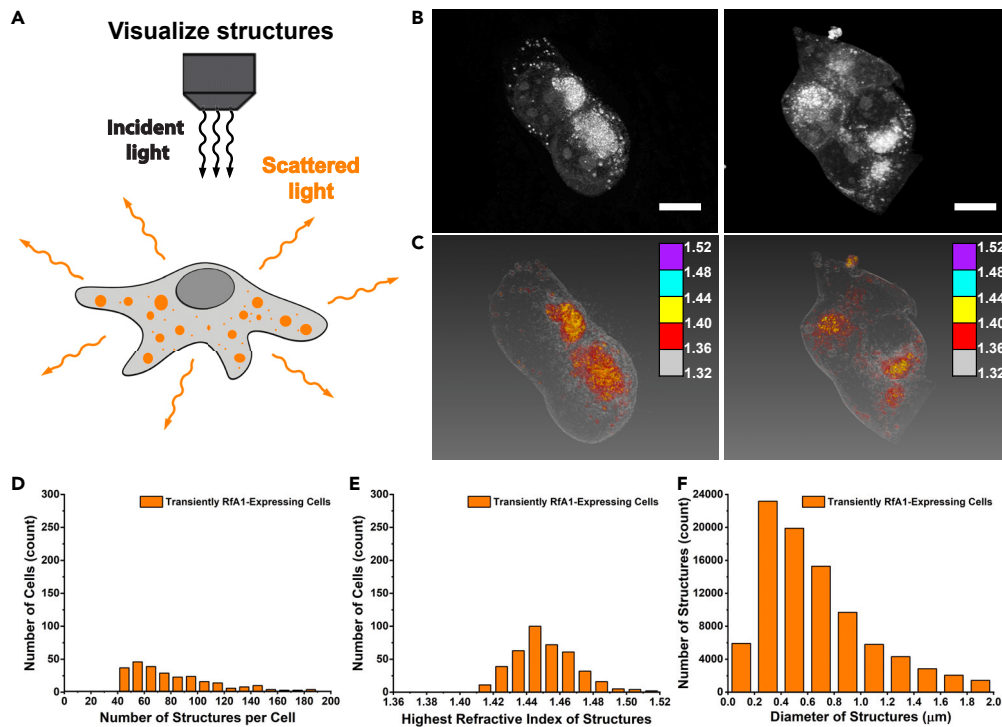
Figure 2. Visualization and quantification of subcellular reflectin-based structures within transiently transfected RfA1-expressing cells

(A) A schematic of the characterization of transiently transfected RfA1-expressing cells with holotomography.

(B) Two representative phase images of transiently transfected RfA1-expressing cells. The brighter regions correspond to higher contrast structures. The scale bars are 10 μm.

(C) Two representative corresponding refractive index maps of transiently transfected RfA1-expressing cells. The colored legends indicate the refractive index ranges (see Videos S1 and S2).

(D) The distribution of the number of reflectin-based structures formed per transiently transfected RfA1-expressing cell. The plot shows values binned to increments of 10.

(E) The distribution of the highest refractive index values for the reflectin-based structures formed per transiently transfected RfA1-expressing cell. The plot shows values binned to increments of 0.01.

(F) The distribution of the diameters for the reflectin-based structures formed in hundreds of transiently transfected RfA1-expressing cells. The plot shows values binned to increments of 0.2 μm.

holotomography, phase contrast microscopy, fluorescence microscopy, and immunofluorescence microscopy imaging data obtained for non-transfected cells indicated comparable characteristics but an absence of RfA1 (Figures S5–S8 and Videos S3 and S4). These experiments together constituted rigorous characterization of our transiently transfected RfA1-expressing human cells and their intracellular proteinaceous structure arrangements.

We next quantitatively evaluated the reflectin-based structure ensembles inside our transiently transfected cells and then leveraged these structures for a ubiquitous cell migration assay. Toward this end, we analyzed our subcellular structures' characteristics with holotomography and conducted *in vitro* scratch assays for the cell populations (see STAR Methods).[22–24] Here, each of the transiently transfected cells typically contained between ∼40 and ∼190 structures with their highest refractive indices between ∼1.41 and ∼1.52 (Figures 2D and 2E). When considered across hundreds of cells, our RfA1-based structures exhibited a broad polydisperse size distribution, with a major peak at a diameter of ∼400 nm and a right tail that approached ∼2000 nm (suggesting that aggregated structures accounted for the larger sizes) (Figure 2F). Notably, the structures' sizes and refractive indices endowed them with a higher contrast relative to their surroundings, which also facilitated the reliable tracking of individual migrating cells with brightfield microscopy over periods of 24 h (Figure S9). By comparison, our non-transfected cells typically contained fewer structures with refractive indices of <1.40, in agreement with the literature,[15,25,26] which precluded tracking of individual migrating cells with brightfield microscopy (Figures S5 and S10). The combined experiments
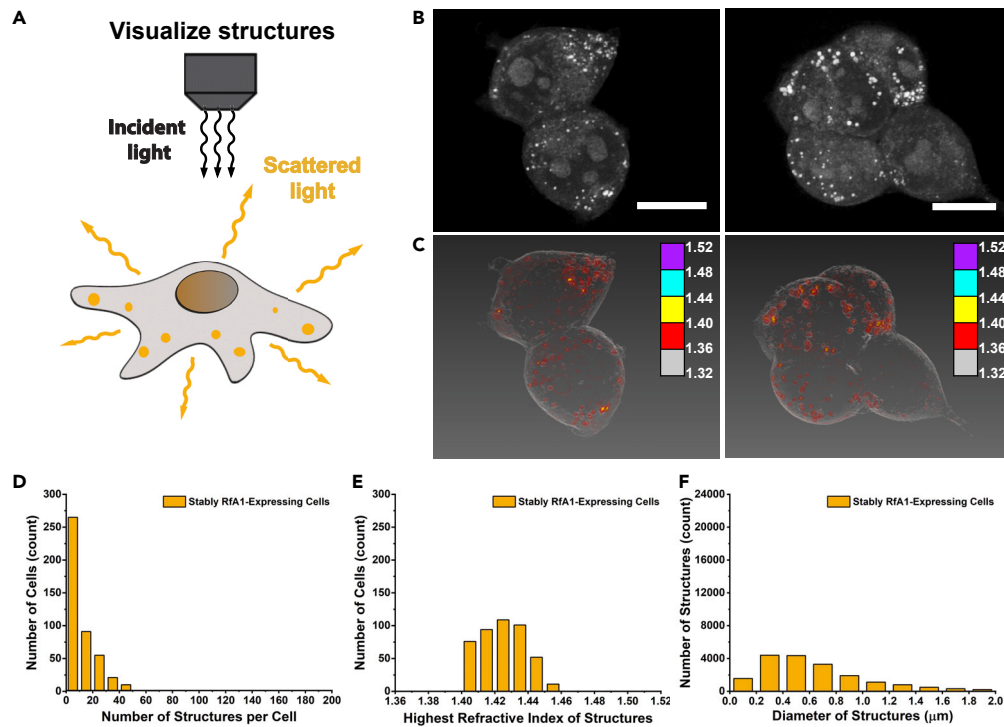
Figure 3. Visualization and quantification of subcellular reflectin-based structures within stably transfected RfA1-expressing cells

(A) A schematic of the characterization of stably transfected RfA1-expressing cells with holotomography.

(B) Two representative phase images of stably transfected RfA1-expressing cells. The brighter regions correspond to higher contrast structures. The scale bars are 10 μm.

(C) Two representative corresponding refractive index maps of stably transfected RfA1-expressing cells. The colored legends indicate the refractive index ranges (see Videos S5 and S6).

(D) The distribution of the number of reflectin-based structures formed per stably transfected RfA1-expressing cell. The plot shows values binned to increments of 10.

(E) The distribution of the highest refractive index values for the reflectin-based structures formed per stably transfected RfA1-expressing cell. The plot shows values binned to increments of 0.01.

(F) The distribution of the diameters for the reflectin-based structures formed in hundreds of stably transfected RfA1-expressing cells. The plot shows values binned to increments of 0.2 μm.

and analyses suggested that reflectin could find applications as a high-contrast reporter for both advanced holotomographic imaging and conventional microscopy imaging techniques.

We continued our efforts by forming and visualizing reflectin-based architectures within stably transfected human cells (Figure 3A). For this purpose, we cultured HEK 293 cells that stably expressed the *D. pealeii* RfA1 isoform via established methods[27–29] and again characterized these cells with a combination of holotomography, phase contrast microscopy, fluorescence microscopy, and immunofluorescence microscopy techniques (see STAR Methods).[15,18–21] First, the representative phase images revealed the presence of seemingly more uniform, i.e., less polydisperse, light-scattering arrangements of spheroidal structures within the cells (Figure 3B). Second, the corresponding holotomographic refractive index maps suggested that the spheroidal structures consisted of RfA1 because of their higher refractive indices relative to the surrounding cytoplasm and organelles (Figure 3C and Videos S5 and S6). Third, the complementary phase contrast microscopy monitoring and cell viability assays indicated that the cells featured epithelial-like morphologies and viabilities that typically exceeded 96%, even after undergoing 24 h of continuous fluorescence/phase contrast imaging (Figures S11 and S12). Fourth, the immunofluorescence images obtained for fixed stably transfected cells further confirmed the presence of expressed RfA1 (Figure S13). In general, the holotomography and microscopy data obtained for our stably transfected cells was comparable but not identical to the analogous data obtained for transiently transfected cells (compare, for example, Figures 2B, 2C, 3B, and 3C).

These experiments together constituted rigorous characterization of our stably transfected RfA1-expressing human cells and their intracellular proteinaceous structure arrangements.

We in turn quantitatively evaluated the reflectin-based structure ensembles inside our stably transfected cells and then leveraged these structures for a ubiquitous biological assay. Toward this end, we analyzed our subcellular structures' characteristics with holotomography and conducted *in vitro* scratch assays for our cell populations (see STAR Methods).[22–24] Here, each of the stably transfected cells typically contained between ∼5 and ∼50 subcellular structures with their highest refractive indices between ∼1.40 and ∼1.46 (Figures 3D and 3E). When considered across hundreds of cells, our RfA1-based structures possessed a narrowed and flattened size distribution, with a peak at diameters of ∼400–∼600 nm and a right tail that approached ∼1800 nm (suggesting that aggregated structures accounted for the larger sizes) (Figure 3F). Notably, the structures' sizes and refractive indices still endowed them with a high contrast relative to their surroundings, which again facilitated the reliable tracking of individual migrating cells with brightfield microscopy over periods of 24 h (Figure S14). When compared to our transiently transfected cells, the stably transfected cells contained ∼3-fold fewer subcellular structures on average but with a ∼2-fold narrower, i.e., better controlled, distribution of the refractive indices (compare, for example, Figures 2D, 2E, 3D, and 3E). The combined experiments and analyses suggested that reflectin could be incorporated as a "more permanent" genetically encoded high-contrast reporter for advanced optical imaging of cells and tissues.

External chemical control over the optical properties of human cells

We extended our efforts by visualizing the effect of a chemical stimulus on the reflectin-based architectures within our transiently transfected cells (Figure 4A). For this purpose, we exposed the transiently transfected RfA1-expressing HEK 293 cells to sodium chloride concentrations that were cytocompatible but still high enough to influence reflectin self-assembly,[15,28,30] and we simultaneously characterized such cells with holotomography in real time (see STAR Methods). Immediately after the application of the chemical stimulus, the representative phase images revealed the expected light-scattering spheroidal structure arrangements within our cells (Figure 4B, left). The corresponding holotomographic refractive index maps established that the spheroidal structures featured higher refractive indices than their surroundings (Figure 4C, left). One hour after the application of the chemical stimulus, the representative phase images revealed changes in the numbers and sizes of the structures within our cells (Figure 4B, right). The corresponding holotomographic refractive index maps indicated that the spheroidal RfA1-based structures now featured even higher refractive indices relative to the surrounding cytoplasm and organelles (Figure 4C, right). Interestingly, the observations were in general agreement with our prior findings for the salt-induced modulation of the optical properties of RfA1-expressing cell cultures.[15] Moreover, the phase images and refractive index maps obtained for non-transfected cells exposed to the same stimulus indicated only subtle number, refractive index, and size changes for their internal structures (Figure S15). These experiments qualitatively demonstrated that the physical characteristics and refractive indices of the proteinaceous structure arrangements inside our engineered cells could be manipulated by an external chemical stimulus.

We next quantitatively evaluated the stimulus-induced changes in the numbers, refractive indices, and size distributions of the reflectin-based structures inside our transiently transfected cells. Toward this end, we analyzed our subcellular structures' characteristics with holotomography before and after exposure to sodium chloride (see STAR Methods). Immediately after the application of the chemical stimulus, a representative transiently transfected cell typically contained between ∼50 and ∼80 structures with highest refractive indices between ∼1.41 and ∼1.43 (Figures 4D and 4E). These subcellular structure ensembles possessed a polydisperse size distribution, with the major peak at a diameter of ∼400 nm and tailing to >1400 nm (corresponding to large aggregates) (Figure 4F). One hour after the application of the chemical stimulus, the same engineered cell typically contained between ∼20 to ∼40 structures with increased highest refractive indices between ∼1.44 and ∼1.46 (Figures 4D and 4E). These subcellular structure ensembles possessed a still polydisperse but substantially shifted size distribution, with the major peak at a diameter of ∼800 nm and tailing to >1400 nm (corresponding to relatively more larger aggregates) (Figure 4F). Notably, the trends quantified for the changes in the physical characteristics of our reflectin-based structures were comparable for cells from multiple different biological and technical experimental repetitions (Table S1). Moreover, the observation of salt-induced self-assembly and aggregation for the structures
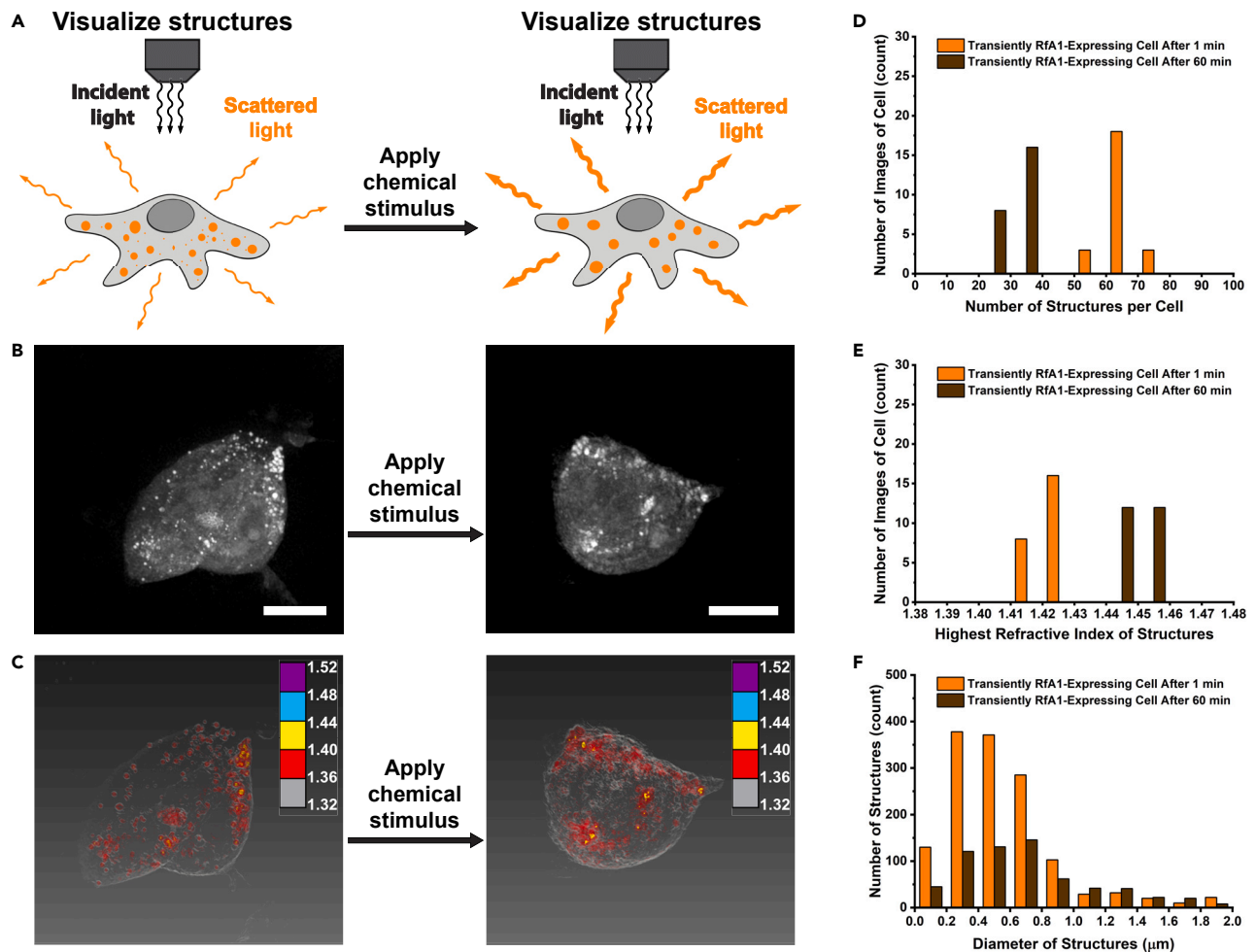
Figure 4. Visualization and quantification of subcellular reflectin-based structures within transiently transfected RfA1-expressing cells before and after the application of a chemical stimulus

(A) A schematic of the characterization of a transiently transfected RfA1-expressing cell with holotomography before and after the application of a chemical stimulus.

(B) Representative phase images obtained for a transiently transfected RfA1-expressing cell before and after the application of a chemical stimulus. The brighter regions correspond to higher contrast structures. The scale bars are 10 μm.

(C) Representative refractive index maps obtained for a transiently transfected RfA1-expressing cell before and after the application of a chemical stimulus. The colored legends indicate the refractive index ranges.

(D) The distribution of the number of reflectin-based structures in a transiently transfected RfA1-expressing cell after 1 min of NaCl exposure (orange) and after 60 min of NaCl exposure (brown). Note that the values were obtained from 48 consecutively collected images, binned to increments of 10, and plotted side-by-side for direct comparison.

(E) The distribution of the highest refractive index values for reflectin-based structures in a transiently transfected RfA1-expressing cell after 1 min of NaCl exposure (orange) and after 60 min of NaCl exposure (brown). Note that the values were obtained from 48 consecutively collected images, binned to increments of 0.01, and plotted side-by-side for direct comparison.

(F) The distribution of the diameters for the reflectin-based structures in a transiently transfected RfA1-expressing cell after 1 min of NaCl exposure (orange) and after 60 min of NaCl exposure (brown). Note that the values were obtained from 48 consecutively collected images, binned to increments of 0.2 μm, and plotted side-by-side for direct comparison.

within our engineered cells was in general agreement with analogous findings for RfA1-based nanoparticles in solution.[15] By comparison, our non-transfected cells typically revealed minor shifts in the numbers, refractive indices, diameters, and aggregation states of their subcellular structures (Figure S15 and Table S2). The combined analysis provided new mechanistic insight into how our engineered cells' reflectin-based structure arrangements and global optical properties could be altered by an external chemical stimulus.
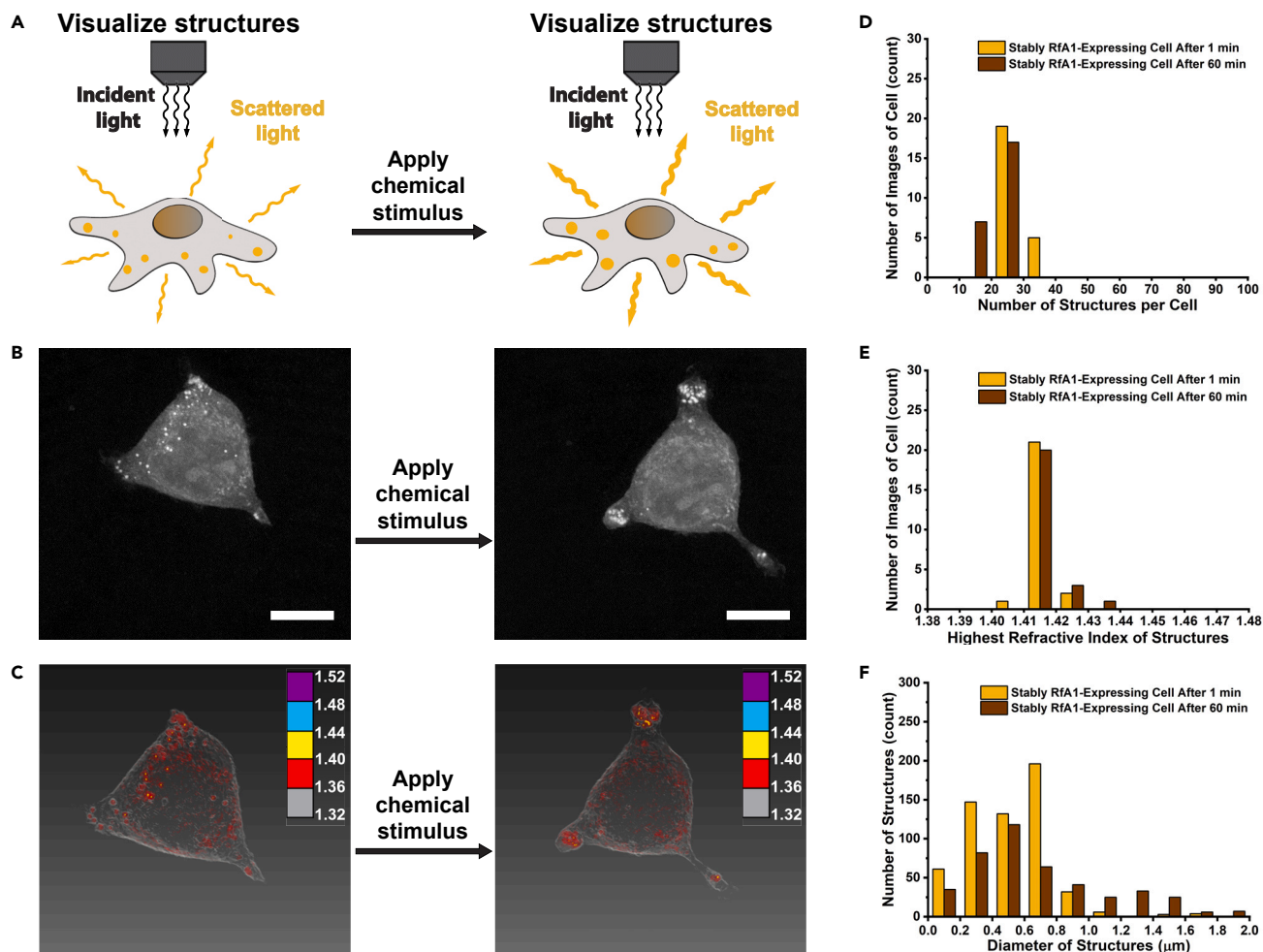
Figure 5. Visualization and quantification of subcellular reflectin-based structures within stably transfected RfA1-expressing cells before and after the application of a chemical stimulus

(A) A schematic of the characterization of a stably transfected RfA1-expressing cell with holotomography before and after the application of a chemical stimulus.

(B) Representative phase images obtained for a stably transfected RfA1-expressing cell before and after the application of a chemical stimulus. The brighter regions correspond to higher contrast structures. The scale bars are 10 μm.

(C) Representative refractive index maps obtained for a stably transfected RfA1-expressing cell before and after the application of a chemical stimulus. The colored legends indicate the refractive index ranges.

(D) The distribution of the number of reflectin-based structures in a stably transfected RfA1-expressing cell after 1 min of NaCl exposure (amber) and after 60 min of NaCl exposure (brown). Note that the values were obtained from 48 consecutively collected images, binned to increments of 10, and plotted side-by-side for direct comparison.

(E) The distribution of the highest refractive index values for reflectin-based structures in a stably transfected RfA1-expressing cell after 1 min of NaCl exposure (amber) and after 60 min of NaCl exposure (brown). Note that the values were obtained from 48 consecutively collected images, binned to increments of 0.01, and plotted side-by-side for direct comparison.

(F) The distribution of the diameters for the reflectin-based structures in a stably transfected RfA1-expressing cell after 1 min of NaCl exposure (amber) and after 60 min of NaCl exposure (brown). Note that the values were obtained from 48 consecutively collected images, binned to increments of 0.2 μm, and plotted side-by-side for direct comparison.

We completed our efforts by visualizing the effect of a chemical stimulus on the reflectin-based architectures within our stably transfected cells (Figure 5A). For this purpose, we exposed the stably transfected RfA1-expressing HEK 293 cells to sodium chloride concentrations that were cytocompatible but still high enough to influence reflectin self-assembly,[15,28,30] and we simultaneously characterized these cells with holotomography in real time (see STAR Methods). Immediately after the application of the chemical stimulus, the representative phase images revealed the expected more uniform, i.e., less polydisperse,

light-scattering spheroidal structure arrangements within our cells (Figure 5B, left). The corresponding holotomographic refractive index maps established that the spheroidal structures featured higher refractive indices than their surroundings (Figure 5C, left). One hour after the application of the chemical stimulus, the representative phase images revealed changes in the numbers and sizes of the structures within our cells (Figure 5B, right). The corresponding holotomographic refractive index maps demonstrated that the spheroidal structures now featured even higher refractive indices relative to the surrounding cytoplasm and organelles (Figure 5C, right). Generally, the stably transfected cells revealed qualitative changes for their proteinaceous structures that were analogous to those found for the transiently transfected cells' structures under the same conditions (compare, for example, Figures 4B, 4C, 5B, and 5C). These experiments qualitatively confirmed that the physical characteristics and refractive indices of the proteinaceous structure arrangements inside our engineered cells could be manipulated by an external chemical stimulus.

We in turn quantitatively evaluated the stimulus-induced changes in the numbers, refractive indices, and size distributions of the reflectin-based structures inside our stably transfected cells. Toward this end, we again analyzed our subcellular structures' characteristics with holotomography before and after exposure to sodium chloride (see STAR Methods). Immediately after the application of the chemical stimulus, a representative stably transfected cell contained between ∼20 and ∼40 structures with highest refractive indices between ∼1.40 and ∼1.43 (Figures 5D and 5E). These subcellular structure ensembles possessed a bell-shaped size distribution, with the major peak at a diameter of ∼800 nm and tailing to >1000 nm (corresponding to large aggregates) (Figure 5F). One hour after the application of the chemical stimulus, the same engineered cell contained between ∼10 and ∼30 subcellular structures with increased highest refractive indices between ∼1.41 and ∼1.44 (Figures 5D and 5E). These subcellular structure ensembles possessed a shifted bell-shaped size distribution, with the major peak at a diameter of ∼600 nm and tailing to >1600 nm (corresponding to relatively more larger aggregates) (Figure 5F). Notably, the trends for the quantified changes in the physical characteristics of our reflectin-based structures were comparable for cells from multiple different biological and technical experimental repetitions (Table S3). When compared to transiently transfected cells under the same conditions, the stably transfected cells generally demonstrated similar but more subtle shifts in the numbers, refractive indices, diameters, and aggregation states of their subcellular structures (compare, for example, Figures 4D–4F and 5D–5F). The combined analysis further reinforced the newfound mechanistic understanding of how our engineered cells' reflectin-based structure arrangements and global optical properties could be altered by an external chemical stimulus.

DISCUSSION

In summary, our expanded ability to incorporate and manipulate reflectin-based structures within mammalian cells holds significance from a fundamental perspective. First, we have generated mammalian cell lines that stably express reflectin and therefore have demonstrated improved genetic control over the formation of subcellular reflectin-based structures. These findings may ultimately further advance the study of reflectins' intrinsic optical properties under physiologically relevant conditions analogous to those in squid skin cells.[4,5] Second, we have shown that the assembly state of the reflectin-based structures formed inside both transiently and stably transfected cells can be reconfigured via a chemical stimulus. These findings validate prior postulates about the mechanisms underpinning the squid leucophore-like tunable light-scattering functionalities of engineered reflectin-expressing mammalian cells, as illustrated in Figure 1C.[15] Such discoveries suggest that our efforts may enable a better understanding of the color- and appearance-changing capabilities of cephalopod skin cells.

Furthermore, our expanded ability to incorporate and interrogate reflectin-based structures within mammalian cells holds significance from an applications perspective. First, we have systematically evaluated the characteristics of the reflectin-based structures formed inside stably and transiently transfected mammalian cells in three dimensions with advanced holotomographic imaging. These findings suggest that reflectins could potentially meet the well-known need for genetically encoded high refractive index biomolecular reporters in quantitative phase microscopy, thus facilitating the visualization of subcellular structures such as organelles and vesicles.[18–20] Second, we have reliably tracked the migration of our engineered cells by means of their high contrast subcellular reflectin-based structures in a scratch assay with standard brightfield microscopy. These findings suggest that reflectins could find applications as genetically encoded high-contrast biomolecular reporters for the straightforward tracking of migration and other cellular-level processes, such as division and differentiation, in two- and three-dimensional cultures.[31–35] Such discoveries point to further exciting opportunities for reflectins as molecular probes in the fields of cell biology and biomedical optics.

Limitations of the study

The major limitation of the study was associated with the technical difficulty of continuously imaging cells for periods of an hour or more after the application of a stimulus. This technical limitation required precise microscope alignment and a low background noise environment.

STAR★METHODS

Detailed methods are provided in the online version of this paper and include the following:

- KEY RESOURCES TABLE
- RESOURCE AVAILABILITY
  - Lead contact
  - Materials availability
  - Data and code availability
- EXPERIMENTAL MODEL AND SUBJECT DETAILS
  - Growth and transient transfection of mammalian cells for phase contrast, immunofluorescence, fluorescence, and brightfield microscopy
  - Growth and stable transfection of mammalian cells for phase contrast, immunofluorescence, fluorescence, and brightfield microscopy
  - Growth and transfection of mammalian cells for holotomography
- METHOD DETAILS
  - Preparation of mammalian cells for immunofluorescence microscopy
  - Preparation of mammalian cells for cell viability assays
  - Preparation of mammalian cells for scratch assays
  - Phase contrast microscopy imaging of live mammalian cells
  - Immunofluorescence microscopy imaging of fixed mammalian cells
  - Fluorescence microscopy imaging of live mammalian cells
  - Brightfield microscopy imaging of live mammalian cells
  - Holotomography imaging of live mammalian cells
  - General statistical analyses and experimental reproducibility

SUPPLEMENTAL INFORMATION

Supplemental information can be found online at https://doi.org/10.1016/j.isci.2023.106854.

AUTHOR CONTRIBUTIONS

A.A.G. conceived the project. G.B. and N.M. performed cell culture and microscopy experiments. G.B. and A.C. developed the protocols and data analysis procedures. G.B. analyzed the data. A.F. assisted with the data analyses. G.B., A.C., A.F., and A.A.G. wrote the manuscript.

DECLARATION OF INTERESTS

A.C. and A.A.G. are listed as authors on an invention disclosure to the University of California, Irvine, which describes the systems and methods for control of refractive index and optical properties in living biological cells.

REFERENCES

1. Mäthger, L.M., Denton, E.J., Marshall, N.J., and Hanlon, R.T. (2009). Mechanisms and behavioural functions of structural coloration in cephalopods. J. R. Soc. Interface 6, 149–163. https://doi.org/10.1098/rsif.2008.0366.focus.

2. Hanlon, R., and Messenger, J. (2018). Cephalopod Behaviour, 2nd Ed. (Cambridge University Press).

3. Chatterjee, A., Norton-Baker, B., Bagge, L.E., Patel, P., and Gorodetsky, A.A. (2018). An introduction to color-changing systems from the cephalopod protein reflectin. Bioinspir. Biomim. 13, 045001. https://doi.org/10.1088/1748-3190/aab804.

4. DeMartini, D.G., Ghoshal, A., Pandolfi, E., Weaver, A.T., Baum, M., and Morse, D.E. (2013). Dynamic biophotonics: female squid exhibit sexually dimorphic tunable leucophores and iridocytes. J. Exp. Biol. 216, 3733–3741. https://doi.org/10.1242/jeb.090415.

5. Mäthger, L.M., Senft, S.L., Gao, M., Karaveli, S., Bell, G.R.R., Zia, R., Kuzirian, A.M., Dennis, P.B., Crookes-Goodson, W.J., Naik, R.R., et al. (2013). Bright white scattering from protein spheres in color changing, flexible cuttlefish skin. Adv. Funct. Mater. 23, 3980–3989. https://doi.org/10.1002/adfm.201203705.

6. DeMartini, D.G. (2014). Molecular and Cellular Mechanisms Controlling Tunable Reflectance. Doctoral dissertation, University of California Santa Barbara (ProQuest Dissertations and Theses Global).

7. Hanlon, R.T., Mäthger, L.M., Bell, G.R.R., Kuzirian, A.M., and Senft, S.L. (2018). White reflection from cuttlefish skin leucophores. Bioinspir. Biomim. 13, 035002. https://doi.org/10.1088/1748-3190/aaa3a9.

8. Phan, L., Kautz, R., Leung, E.M., Naughton, K.L., Van Dyke, Y., and Gorodetsky, A.A. (2016). Dynamic materials inspired by cephalopods. Chem. Mater. 28, 6804–6816. https://doi.org/10.1021/acs.chemmater.6b01532.

9. Tadepalli, S., Slocik, J.M., Gupta, M.K., Naik, R.R., and Singamaneni, S. (2017). Bio-optics and bio-inspired optical materials. Chem. Rev. 117, 12705–12763. https://doi.org/10.1021/acs.chemrev.7b00153.

10. Isapour, G., and Lattuada, M. (2018). Bioinspired stimuli-responsive color-changing systems. Adv. Mater. 30, 1707069. https://doi.org/10.1002/adma.201707069.

11. Dennis, P.B., Onderko, E.L., Slocik, J.M., Bird, L.J., Phillips, D.A., Crookes-Goodson, W.J., and Glaven, S.M. (2020). Proteins for bioinspired optical and electronic materials. MRS Bull. 45, 1027–1033. https://doi.org/10.1557/mrs.2020.297.

12. Burgos-Morales, O., Gueye, M., Lacombe, L., Nowak, C., Schmachtenberg, R., Hörner, M., Jerez-Longres, C., Mohsenin, H., Wagner, H.J., and Weber, W. (2021). Synthetic biology as driver for the biologization of materials sciences. Mater. Today Bio. 11, 100115. https://doi.org/10.1016/j.mtbio.2021.100115.

13. Dou, S., Xu, H., Zhao, J., Zhang, K., Li, N., Lin, Y., Pan, L., and Li, Y. (2021). Bioinspired microstructured materials for optical and thermal regulation. Adv. Mater. 33, 2000697. https://doi.org/10.1002/adma.202000697.

14. Yang, J., Zhang, X., Zhang, X., Wang, L., Feng, W., and Li, Q. (2021). Beyond the visible: bioinspired infrared adaptive materials. Adv. Mater. 33, 2004754. https://doi.org/10.1002/adma.202004754.

15. Chatterjee, A., Cerna Sanchez, J.A., Yamauchi, T., Taupin, V., Couvrette, J., and Gorodetsky, A.A. (2020). Cephalopod-inspired optical engineering of human cells. Nat. Commun. 11, 2708. https://doi.org/10.1038/s41467-020-16151-6.

16. Phan, L., Kautz, R., Arulmoli, J., Kim, I.H., Le, D.T.T., Shenk, M.A., Pathak, M.M., Flanagan, L.A., Tombola, F., and Gorodetsky, A.A. (2016). Reflectin as a material for neural stem cell growth. ACS Appl. Mater. Interfaces 8, 278–284. https://doi.org/10.1021/acsami.5b08717.

17. Kautz, R., Phan, L., Arulmoli, J., Chatterjee, A., Kerr, J.P., Naeim, M., Long, J., Allevato, A., Leal-Cruz, J.E., Le, L., et al. (2020). Growth and spatial control of murine neural stem cells on reflectin films. ACS Biomater. Sci. Eng. 6, 1311–1320. https://doi.org/10.1021/acsbiomaterials.9b00824.

18. Park, Y., Depeursinge, C., and Popescu, G. (2018). Quantitative phase imaging in biomedicine. Nat. Photon. 12, 578–589. https://doi.org/10.1038/s41566-018-0253-x.

19. Balasubramani, V., Kuś, A., Tu, H.-Y., Cheng, C.-J., Baczewska, M., Krauze, W., and Kujawińska, M. (2021). Holographic tomography: techniques and biomedical applications. Appl. Opt. 60, 65–80. https://doi.org/10.1364/AO.416902.

20. Kim, D., Lee, S., Lee, M., Oh, J., Yang, S.-A., and Park, Y. (2021). Holotomography: refractive index as an intrinsic imaging contrast for 3-D label-free live cell imaging. Adv. Exp. Med. Biol. 1310, 211–238. https://doi.org/10.1007/978-981-33-6064-8_10.

21. Umerani, M.J., Pratakshya, P., Chatterjee, A., Cerna Sanchez, J.A., Kim, H.S., Ilc, G., Kovačič, M., Magnan, C., Marmiroli, B., Sartori, B., et al. (2020). Structure, self-assembly, and properties of a truncated reflectin variant. Proc. Natl. Acad. Sci. USA 117, 32891–32901. https://doi.org/10.1073/pnas.2009044117.

22. Liang, C.-C., Park, A.Y., and Guan, J.-L. (2007). In vitro scratch assay: a convenient and inexpensive method for analysis of cell migration in vitro. Nat. Protoc. 2, 329–333. https://doi.org/10.1038/nprot.2007.30.

23. Pijuan, J., Barceló, C., Moreno, D.F., Maiques, O., Sisó, P., Marti, R.M., Macià, A., and Panosa, A. (2019). In vitro cell migration, invasion, and adhesion assays: from cell imaging to data analysis. Front. Cell Dev. Biol. 7, 107. https://doi.org/10.3389/fcell.2019.00107.

24. Bobadilla, A.V.P., Arévalo, J., Sarró, E., Byrne, H.M., Maini, P.K., Carraro, T., Balocco, S., Meseguer, A., and Alarcón, T. (2019). In vitro cell migration quantification method for scratch assays. J. R. Soc. Interface 16, 20180709. https://doi.org/10.1098/rsif.2018.0709.

25. Kim, K., Lee, S., Yoon, J., Heo, J., Choi, C., and Park, Y. (2016). Three-dimensional label-free imaging and quantification of lipid droplets in live hepatocytes. Sci. Rep. 6, 36815. https://doi.org/10.1038/srep36815.

26. Park, S., Ahn, J.W., Jo, Y., Kang, H.-Y., Kim, H.J., Cheon, Y., Kim, J.W., Park, Y., Lee, S., and Park, K. (2020). Label-free tomographic imaging of lipid droplets in foam cells for machine-learning-assisted therapeutic evaluation of targeted nanodrugs. ACS Nano 14, 1856–1865. https://doi.org/10.1021/acsnano.9b07993.

27. Hacker, D.L., and Balasubramanian, S. (2016). Recombinant protein production from stable mammalian cell lines and pools. Curr. Opin. Struct. Biol. 38, 129–136. https://doi.org/10.1016/j.sbi.2016.06.005.

28. Dyson, M.R. (2016). Fundamentals of expression in mammalian cells. Adv. Exp. Med. Biol. 896, 217–224. https://doi.org/10.1007/978-3-319-27216-0_14.

29. González-Domínguez, I., Puente-Massaguer, E., Lavado-García, J., Cervera, L., and Gòdia, F. (2022). Micrometric DNA/PEI polyplexes correlate with higher transient Gene expression yields in HEK 293 cells. N. Biotechnol. 68, 87–96. https://doi.org/10.1016/j.nbt.2022.02.002.

30. Dmitrieva, N.I., and Burg, M.B. (2007). High NaCl promotes cellular senescence. Cell Cycle 6, 3108–3113. https://doi.org/10.4161/cc.6.24.5084.

31. Ong, J.Y., and Torres, J.Z. (2019). Dissecting the mechanisms of cell division. J. Biol. Chem. 294, 11382–11390. https://doi.org/10.1074/jbc.AW119.008149.

32. Yamada, K.M., and Sixt, M. (2019). Mechanisms of 3D cell migration. Nat. Rev. Mol. Cell Biol. 20, 738–752. https://doi.org/10.1038/s41580-019-0172-9.

33. Wu, X., Su, J., Wei, J., Jiang, N., and Ge, X. (2021). Recent advances in three-dimensional stem cell culture systems and applications. Stem Cells Int. 2021, 9477332. https://doi.org/10.1155/2021/9477332.

34. Pawluchin, A., and Galic, M. (2022). Moving through a changing world: single cell migration in 2D vs. 3D. Front. Cell Dev. Biol. 10, 1080995. https://doi.org/10.3389/fcell.2022.1080995.

35. Suarez-Martinez, E., Suazo-Sanchez, I., Celis-Romero, M., and Carnero, A. (2022). 3D and organoid culture in Research: physiology, hereditary genetic diseases and cancer. Cell Biosci. 12, 39. https://doi.org/10.1186/s13578-022-00775-w.

STAR★METHODS

KEY RESOURCES TABLE

REAGENT or RESOURCE	SOURCE	IDENTIFIER
Recombinant DNA		
RfA1 Plasmid	ATUM	Gene ID: 511675
RfA1-IRES-Puro Plasmid	ATUM	Gene ID: 330001
Antibodies		
Polyclonal Chicken Anti-reflectin Primary Antibody	Aves	N/A
Goat Anti-chicken IgY (H + L) Secondary Antibody, Alexa Fluor™ 647	Invitrogen	A-21449
Chemicals, peptides, and recombinant proteins		
Fetal Bovine Serum (FBS)	Gibco	A3160502
Minimum Essential Media (MEM)	Gibco	11-095-080
Lipofectamine™ 2000	Invitrogen	11-668-019
Triton™ X-100	ThermoFisher	PI28314
BlokHen®	Aves	BH-1001
Puromycin Dihydrochloride	Gibco	A1113803
ActinRed™ 555 ReadyProbes™ Reagent	Invitrogen	R37112
4′,6-Diamidino-2-Phenylindole (DAPI)	Invitrogen	D1306
Dulbecco's Phosphate-Buffered Saline (DPBS)	Gibco	14-190-250
4% Paraformaldehyde	Electron Microscopy Sciences	50-259-99
Critical commercial assays		
ReadyProbes™ Cell Viability Imaging Kit, Blue/Green	ThermoFisher	R37609
Experimental models: Cell lines		
Human Embryonic Kidney (HEK) 293 cells	ATCC	CRL-1573
Software and algorithms		
OriginPro 2023	OriginLab	N/A
TomoStudio v. 2.7.43	Tomocube	N/A
ImageJ v. 1.53	National Institutes of Health	N/A
Zen Black v. 2.3	Zeiss	N/A
Zen Blue v. 3.2	Zeiss	N/A
Lipid Analysis v. 1.2.1	Tomocube	N/A
Gen5	BioTek	N/A

RESOURCE AVAILABILITY

Lead contact

Further information and requests for resources and reagents should be directed to the lead contact, Alon A. Gorodetsky (alon.gorodetsky@uci.edu).

Materials availability

Plasmids and HEK 293 cells used in this study were sourced commercially. All reagents and materials are available from the vendors described in the key resources table. Stably transfected RfA1-expressing cell lines generated in this study may be available from the lead contact upon reasonable request with a completed Materials Transfer Agreement.

Data and code availability

● The data reported in this paper will be shared by the lead contact upon reasonable request.

- This paper does not report original code.

- Any additional information required to evaluate the data reported in this paper is available from the lead contact upon reasonable request.

EXPERIMENTAL MODEL AND SUBJECT DETAILS

Growth and transient transfection of mammalian cells for phase contrast, immunofluorescence, fluorescence, and brightfield microscopy

The human embryonic kidney (HEK) 293 cells were grown and transiently transfected according to reported protocols.[15] Initially, a vector construct encoding for the independent expression of N-terminal histidine-tagged RfA1 (Genbank: ACZ57764.1) was designed with ATUM Gene Designer Software. The vector contained 5′UTR regions downstream of a simian virus 40 (SV40) promoter and enhancer, a standard origin of replication derived from pBR322, a polyadenylation signal to aid in the termination of transcription, and cDNA encoding for the protein of interest. The HEK 293 cells (ATCC, CRL-1573, authenticated for correct identification by the commercial vendor) were typically seeded at a density of ~30,000 cells/cm^2 on fibronectin-coated 3-well glass-bottom dishes (Ibidi) in Minimal Essential Medium (MEM) supplemented with Earle's salts and 10% fetal bovine serum (FBS) (Gibco), and they were cultured for 24 h at a temperature of 37 °C and under 5% CO_2. The media was then swapped for MEM supplemented with Earle's salts but lacking FBS, and the cells were incubated for 24 h with a transfection reagent mixture containing Lipofect-amine 2000 (Invitrogen) and the above vector construct. The non-transfected cell cultures were grown under identical conditions but in the absence of the transfection reagent mixture. The resulting transiently RfA1-expressing or non-transfected cells were characterized with phase contrast, immunofluorescence, fluorescence, and brightfield microscopy.

Growth and stable transfection of mammalian cells for phase contrast, immunofluorescence, fluorescence, and brightfield microscopy

The HEK 293 cells were cultured and stably transfected by modifying reported protocols.[27–29] Initially, a vector construct encoding for the co-expression of both N-terminal histidine-tagged RfA1 and Puromycin N-acetyltransferase (PAC) was designed with ATUM Gene Designer Software, with the expression of the latter mediated by an internal ribosome entry site (IRES) from the encephalomyocarditis virus. The vector contained 5′UTR regions downstream of a simian virus 40 (SV40) promoter and enhancer, a standard origin of replication derived from pBR322, a polyadenylation signal to aid in the termination of transcription, and cDNA encoding for the protein of interest. The HEK 293 cells (ATCC, CRL-1573) were typically seeded at a density of ~30,000 cells/cm^2 in T-75 flasks (Thermoscientific, Nunc EasYFlask) in MEM supplemented with Earle's salts and 10% FBS (Gibco) at a temperature of 37°C and under 5% CO_2. When the cells reached ~80% confluency, the medium was swapped for MEM supplemented with Earle's salts but lacking FBS, and the cells were incubated for 24 h with a transfection reagent mixture containing Lipofectamine 2000 (Invitrogen) and the above vector construct. The cells were subsequently maintained over at least 4 passages in MEM media containing 4 μg/ml of puromycin dihydrochloride in 4-(2-hydroxyethyl)-1-piperazineethanesulfonic acid (HEPES) buffer (Gibco). The resulting stably RfA1-expressing cells were characterized with phase contrast, immunofluorescence, fluorescence, and brightfield microscopy.

Growth and transfection of mammalian cells for holotomography

The transiently RfA1-expressing, stably RfA1-expressing, and non-transfected cells were prepared for imaging according to standard protocols. First, the various cells were seeded at densities of ~30,000 cells cm^{-2} onto fibronectin-coated glass-bottom TomoDishes (Tomocube) and were cultured in FBS-containing media for 24 h hours. Next, the cells were either transfected with a vector encoding for the expression of RfA1 in FBS-free media for 24 hours (transiently transfected cells), cultured in FBS-free puromycin-supplemented media for 24 hours (stably transfected cells), or cultured in FBS-free media for 24 hours (non-transfected cells). Last, the various cells were again cultured in FBS-containing media for another 24 hours. The resulting transfected or non-transfected cells were imaged via holotomography.

METHOD DETAILS

Preparation of mammalian cells for immunofluorescence microscopy

The transiently RfA1-expressing, stably RfA1-expressing, and non-transfected cells were fixed and immunolabelled according to standard protocols.[15] First, the transfected or non-transfected cells were fixed

with 4% paraformaldehyde (PFA) (Electron Microscopy Sciences) in Dulbecco's phosphate buffered saline (DPBS), permeabilized with 0.1% Triton-X 100 in DPBS, and blocked with 10% BlokHen (AVES) in DPBS. Next, the fixed cells were incubated with a polyclonal chicken anti-reflectin primary antibody (AVES) solution (prepared at a ratio of 1:1000 in PBS containing 1% BSA). In turn, the cells were thoroughly washed with PBS and incubated with a goat anti-chicken IgY (H+L) Alexa Fluor 647 secondary antibody (Invitrogen) solution (prepared at a ratio of 1:500 in PBS containing 1% BSA). Subsequently, the cells were washed with DPBS and incubated with both the nuclear stain 4′,6′-diamidino-2-phenylindole (DAPI) (Invitrogen) and the actin stain phalloidin conjugated to Rhodamine (Invitrogen, ActinRed 555 Ready Probes). Finally, the cells were washed with PBS and treated with anti-fade mounting media (Ibidi). Here, the polyclonal chicken anti-reflectin primary antibody demonstrated specificity similar to that reported for a previously validated polyclonal rabbit anti-reflectin primary antibody.[15] The resulting immunolabelled transfected and non-transfected and cells were imaged with confocal fluorescence microscopy.

Preparation of mammalian cells for cell viability assays

The transiently RfA1-expressing, stably RfA1-expressing, and non-transfected cells were labeled according to standard protocols. First, the cells were incubated at a temperature of 37°C and under 5% CO_2 for 24 hours. Next, the cells were washed with DPBS and incubated with both the nuclear stain Hoechst 33342 and the nucleic acid stain SYTOX (ThermoFisher, ReadyProbes Cell Viability Imaging Kit, Blue/Green). The resulting transfected or non-transfected cells were imaged with fluorescence microscopy.

Preparation of mammalian cells for scratch assays

The transiently RfA1-expressing, stably RfA1-expressing, and non-transfected cells were prepared for the assays according to standard protocols.[22–24] First, the various cells were seeded at densities of ~90,000 cells cm^{-2} onto fibronectin-coated glass-bottom 24-well plates (Costar) and cultured in FBS-containing media for 24 hours. Next, the cells were either transfected with a vector encoding for the expression of RfA1 in FBS-free media for 24 hours (transiently transfected cells), cultured in FBS-free puromycin-supplemented media for 24 hours (stably transfected cells), or cultured in FBS-free media for 24 hours (non-transfected cells). Last, the various cells were again cultured in FBS-containing media for another 24 hours. The resulting transfected or non-transfected cell cultures were imaged with brightfield microscopy.

Phase contrast microscopy imaging of live mammalian cells

The transiently RfA1-expressing, stably RfA1-expressing, and non-transfected cells were imaged using an EVOS M5000 Imaging System (ThermoScientific). During routine imaging, the phase contrast microscopy images were recorded as individual snapshots for the transiently transfected RfA1-expressing, stably transfected RfA1-expressing, and non-transfected cells in FBS-containing MEM cell culture media. During time-dependent imaging, the phase contrast microscopy images were captured together with fluorescence microscopy images every 15 seconds over a period of 24 hours as multiple snapshots for the transiently RfA1-expressing, stably RfA1-expressing, and non-transfected cells in FBS-containing MEM cell culture media. The phase contrast microscopy images were processed with ImageJ (v. 1.53).

Immunofluorescence microscopy imaging of fixed mammalian cells

The fixed and immunolabeled transiently RfA1-expressing, stably RfA1-expressing, and non-transfected cells were imaged with a Zeiss LSM 780 confocal microscope equipped with a Nikon GaAsP detector and an Argon laser. The fluorescence excitation wavelengths were 405, 532, or 633 nm. The resulting confocal images were captured with ZEN Black software (v 2.3) and analyzed with the Zen Blue software (v. 3.2).

Fluorescence microscopy imaging of live mammalian cells

The live stained transiently RfA1-expressing, stably RfA1-expressing, and non-transfected cells were imaged using an EVOS M5000 Imaging System (ThermoScientific). During routine imaging, the fluorescence microscopy images were recorded as individual snapshots for the transiently transfected RfA1-expressing, stably transfected RfA1-expressing, and non-transfected cells in FBS-containing MEM cell culture media. During time-dependent imaging, the fluorescence microscopy images were captured together with phase contrast microscopy images every 15 seconds over a period of 24 hours as multiple snapshots for the transiently RfA1-expressing, stably RfA1-expressing, and non-transfected cells in FBS-containing MEM cell

culture media. The fluorescence excitation wavelengths were 357 nm, 470 nm, or 531 nm. The fluorescence microscopy images were analyzed with ImageJ (v. 1.53).

Brightfield microscopy imaging of live mammalian cells

The transiently RfA1-expressing, stably RfA1-expressing, and non-transfected cell cultures featuring scratches were imaged using a Cytation 5 Cell Imaging Multimode Reader (BioTek). During routine imaging, the brightfield microscopy images were recorded as individual snapshots for the transiently transfected RfA1-expressing, stably transfected RfA1-expressing, and non-transfected cells in FBS-containing MEM cell culture media. During time-dependent imaging, the brightfield microscopy images were captured every 2 minutes over a period of 24 hours as multiple snapshots for the transiently RfA1-expressing, stably RfA1-expressing, and non-transfected cells in FBS-containing MEM cell culture media. The resulting images were captured with Gen5 software (BioTek) and processed with ImageJ (v. 1.53).

Holotomography imaging of live mammalian cells

The transiently RfA1-expressing, stably RfA1-expressing, and non-transfected cells were imaged using an HT-2 Holotomographic Microscope (Tomocube) equipped with a 532 nm laser.[18–20] During routine imaging, the phase images and three-dimensional refractive index maps were recorded as individual snapshots for the transiently transfected RfA1-expressing, stably transfected RfA1-expressing, and non-transfected cells in FBS-containing MEM cell culture media. During time-dependent imaging with and without a chemical stimulus, the phase images and three-dimensional refractive index maps were captured every 5 seconds over a period of an hour as multiple snapshots for the transiently transfected RfA1-expressing, stably transfected RfA1-expressing, and non-transfected cells in FBS-containing MEM cell culture media either without or with the addition of 100 mM NaCl. Note, that this concentration has been shown to modulate RfA1 nanoparticle self-assembly *in vitro*[15] but does not compromise cell viability.[28,30] Note also that NaCl concentrations of <50 mM did not induce obvious changes in the numbers, refractive indices, diameters, and aggregation states of the subcellular reflectin-based structures. For all experiments, the cells were housed in a commercial heating chamber (Tomocube, TomoChamber) for which the temperature was maintained at 37°C. The phase images and refractive index maps were captured and analyzed with the TomoStudio (v. 2.7.43) software to extract the refractive index values for the protein-based structures and analyzed with the Tomocube Lipid Analysis software (v. 1.2.1) to extract the numbers and sizes for the protein-based structures.

General statistical analyses and experimental reproducibility

The statistical analyses were performed using OriginPro software (OriginLab). The data were expressed as the mean ± standard deviation (where appropriate). A minimum of three biologically independent experiments were performed under all experimental conditions. Representative phase contrast microscopy images from at least n = 3 biological replicates are shown in Figures S2, S6, and S11. Representative fluorescence microscopy images from at least n = 3 biological replicates are shown in Figures S3, S7, and S12. Representative immunofluorescence microscopy images from at least n = 3 biological replicates are shown in Figures S4, S8, and S13. Representative brightfield microscopy images from at least n = 3 biological replicates are shown in Figures S9, S10, and S14. Representative holotomography phase images and refractive index maps from at least n = 3 biological replicates are shown in Figures 2, 3, and S5. Representative holotomography phase images and refractive index maps before and after a chemical stimulus from at least n = 3 biological replicates are shown in Figures 4, 5, and S15.